ICASSP 2025 - 2025 IEEE International Conference on Acoustics, Speech and Signal Processing (ICASSP) | 979-8-3503-6874-1/25/$31.00 ©2025 IEEE | DOI: 10.1109/ICASSP49660.2025.10890350

Integrated Interpolation and Matrix Completion for Radio Map Estimation: A Convex Optimization Approach

Hongcheng Dong*, Wenqiang Pu*, Rui Zhou*, Xiao Fu†, Feng Yin*
*Shenzhen Research Institute of Big Data, The Chinese University of Hong Kong, Shenzhen, Guangdong, China
†School of Electrical Engineering and Computer Science, Oregon State University, Corvallis, OR, USA
Email: hongchengdong1@link.cuhk.edu.cn, {wpu, rui.zhou}@sribd.cn, xiao.fu@oregonstate.edu, yinfeng@cuhk.edu.cn

***Abstract*—Radio map estimation (RME) is crucial for effective planning and optimization of wireless networks. Traditional approaches such as interpolation excel at capturing local smoothness in densely populated data but struggle with sparse or irregular data. Conversely, matrix completion (MC) approaches utilize global structures but require huge number of samples and may produce non-smooth estimates. To integrate these strengths, we propose a convex optimization approach for RME (IIMC-RME) that merges interpolation with MC. This approach formulates the RME task as a low-rank MC problem constrained by interpolated results. Additionally, we have developed a convergent algorithm utilizing the alternating direction method of multipliers (ADMM) to efficiently solve the IIMC-RME problem. Experimental evaluations on both synthetic and real-world datasets have shown that IIMC-RME surpasses existing approaches, thereby achieving superior accuracy in RME.**

***Index Terms*—Radio Map Estimation, Interpolation, Matrix Completion, Integrated Interpolation and Matrix Completion**

I. Introduction

Radio map is a spatial representation that shows the radio signal strength or other relevant properties across a specific geographical area. It has become an essential tool for optimizing wireless network operations and enhancing various communication processes, such as improving positioning accuracy [1], supporting unmanned aerial vehicle (UAV) route planning [2] and optimizing resource allocation in dense network environments [3]. Due to the prohibitively high costs associated with measuring radio signals at every position in practical implementations, researchers have developed radio map estimation (RME) approaches [4]–[6], which aim to reconstruct complete radio maps by utilizing spatially sampled measurements.

Recent research on RME predominantly utilizes data-driven approaches which can be divided into two categories. Deep neural network (DNN)-based approaches such as RadioUNet [7], PLNet [8], and FadeNet [9] learn propagation rules and environment effects on radio map but require extensive training data and are often sensitive to the mismatch between training and real-world environment. In contrast, other data-driven techniques, such as matrix completion (MC) and interpolation approaches, only require observations of the current radio map to perform RME, without the need for additional data for training. Specifically, MC strives to reconstruct a low-rank matrix from a partially observed matrix, often employing nuclear norm minimization (NNM) [10] [1]. Interpolation approaches, meanwhile, predict missing values in the radio map by fitting a smooth function to observed data points, with common techniques including linear interpolation (LERP) [13] and k-nearest neighbor Gaussian process regression (KNN-GPR) [14].

MC effectively leverages the global low-rank structure of the radio map but typically requires more samples [15] comparing with DNN-based approaches and may produce non-smooth estimates [16]. In contrast, interpolation methods excel with dense, regularly spaced data, but their accuracy significantly decreases with sparse or irregular data due to their heavy dependence on the distribution and density of observed points [17, Section 6]. To integrate both approaches, [18] enriches the observation matrix through interpolation approaches and then performs MC, [19] employs interpolation as refinement in tensor completion for enhancing RME, and [20] integrates interpolation approaches directly into the MC objective function. These approaches represent a direct integration of interpolation with MC. However, the interpolation approach's reliance on the local smoothness of the radio map limits its effectiveness to certain regions, making it challenging to directly integrate with MC.

In this paper, therefore, we consider to integrate the advantages of both interpolation and MC to overcome this limitation. First, we propose a convex formulation, IIMC-RME, that integrates interpolation within a low-rank matrix framework. Second, we introduce an algorithm based on the alternating direction method of multipliers (ADMM) [21] to efficiently solve the IIMC-RME problem. Finally, our results on both synthetic and real-world datasets demonstrate that IIMC-RME outperforms all existing MC and interpolation approaches.

This work was supported in part by the National Nature Science Foundation of China (NSFC) under Grant 62101350, and Grant 62201362, and in part by the Shenzhen Science and Technology Program under Grant No. RCBS20221008093126071. The work of X. Fu was supported in part by the National Science Foundation (NSF) under Projects NSF ECCS-2024058 and NSF CCF-2210004. The work of F. Yin was supported by the Shenzhen Science and Technology Program under Grant No. JCYJ20220530143806016.

[1] Radio map itself is not a low-rank matrix, but has many small singular values. Several approaches [11], [12] have exploited such structure and study RME from low rank matrix completion view.

II. Problem Formulation

A. Problem Statement

RME aims to reconstruct a complete representation of radio signal strengths over a specific area based on partially observed data. Let the observed samples be collected in a matrix $\mathbf{Y} \in \mathbb{R}^{m\times n}$, where $\mathbf{\Omega} \in \mathbb{R}^{m\times n}$ is a binary matrix indicating the availability of data. Specifically, $\mathbf{\Omega}_{ij} = 1$ if the entry in $\mathbf{Y}$ is observed, or $\mathbf{\Omega}_{ij} = 0$ otherwise. The objective of the RME problem is to reconstruct a complete matrix $\mathbf{X}$ that matches the observed entries in $\mathbf{Y}$ as close as possible. This problem can be generally formalized as:

$$\text{Find } \mathbf{X} \quad \text{s.t.}\, \mathbf{P}_{\mathbf{\Omega}}(\mathbf{X}) = \mathbf{P}_{\mathbf{\Omega}}(\mathbf{Y}), \tag{1}$$

where $\mathbf{P}_{\mathbf{\Omega}}(\mathbf{Y}) = \mathbf{\Omega} \odot \mathbf{Y}$, $\odot$ denotes the Hadamard product.

B. Background

To effectively address the RME problem as defined in (1), it is crucial to establish a suitable criterion for the objective 'Find $\mathbf{X}$'. In the literature, two primary approaches have been widely used: MC and interpolation. For MC, [10] proposes using NNM to promote low-rank solutions. On the other hand, interpolation-based approaches focus on estimating missing values through various interpolation techniques. For example, [13] use LERP and [14] apply KNN-GPR. Below we briefly review these two types of approaches.

Matrix Completion Approach: Such approach has been derived based on an important numerical fact that the radio map has inherently global low-rank structures, see the example in Figure 1. Based on this finding, the MC approach can be formulated as [15]:

$$\min_{\mathbf{X}} \text{rank}(\mathbf{X}) \quad \text{s.t.}\, \mathbf{P}_{\mathbf{\Omega}}(\mathbf{X}) = \mathbf{P}_{\mathbf{\Omega}}(\mathbf{Y}). \tag{2}$$

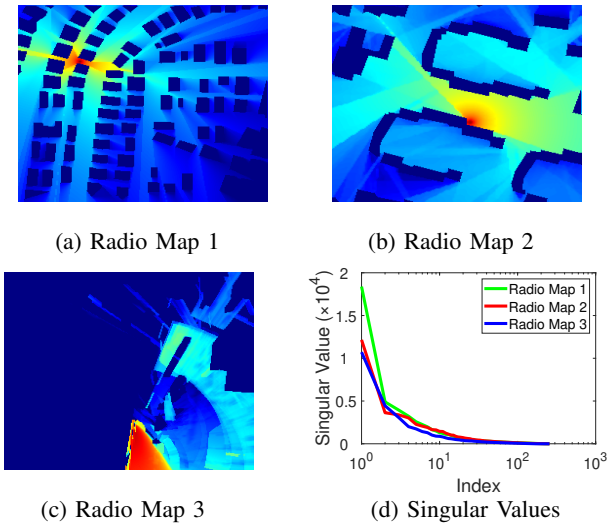

(a) Radio Map 1 (b) Radio Map 2 (c) Radio Map 3 (d) Singular Values

Fig. 1: Three different types of radio maps, with the first two examples taken from [22] and the third from [23], and their corresponding singular values, where blue represents the minimum pixel value (0) and red represents the maximum pixel value (255) in subfigures (a) - (c).

Interpolation based Approach: The motivation is based on the radio signal propagation rule that signal power diminishes with distance, suggesting that signal strength changes smoothly across space. The general formulation of the interpolation approach can be formulated as:

$$\mathbf{Z} = \text{INTP}(\mathbf{P}_{\mathbf{\Omega}}(\mathbf{Y}), \mathbf{\Omega}), \tag{3}$$

where INTP denote an arbitrary interpolation approach.

Hybrid Approach: MC approach leverages global low-rank structure but requires many samples and often yields non-smooth estimates. Interpolation works well with dense data but loses accuracy on sparse or irregular data due to the dependence on the distribution of observed points. To integrate both approaches, [18] exploits interpolation approaches to enrich the observation matrix then perform MC, [19] uses interpolation as refinement in tensor completion to enhance RME, and [20] integrates interpolation directly into the MC objective. However, the interpolation approach's reliance on the local smoothness of the radio map limits its effectiveness to certain regions, making it challenging to directly integrate with MC.

C. Proposed Formulation

To integrate the localized effects of interpolation with the global structure of MC, we propose the following formulation:

$$\begin{aligned} \min_{\mathbf{X}} \quad & \text{rank}(\mathbf{X}) \\ \text{s.t.} \quad & \mathbf{P}_{\mathbf{\Omega}}(\mathbf{X}) = \mathbf{P}_{\mathbf{\Omega}}(\mathbf{Y}), \\ & \mathbf{X} \in \mathcal{C}(\mathbf{Z}), \quad \mathbf{Z} = \text{INTP}(\mathbf{P}_{\mathbf{\Omega}}(\mathbf{Y}), \mathbf{\Omega}), \end{aligned} \tag{4}$$

where $\mathcal{C}$ is a closed set depending on $\mathbf{Z}$. The above formulation constrains the estimated value $\mathbf{X}$ within a closed set $\mathcal{C}(\mathbf{Z})$ that is related to the interpolation results $\mathbf{Z}$. In this paper, we choose weighted nuclear norm minimization (WNNM) [24] as the objective and KNN [25] as the interpolation approach, then the resulting optimization problem becomes:

$$\begin{aligned} \min_{\mathbf{X}} \quad & \|\mathbf{X}\|_{\mathbf{w},*} \\ \text{s.t.} \quad & \mathbf{P}_{\mathbf{\Omega}}(\mathbf{X}) = \mathbf{P}_{\mathbf{\Omega}}(\mathbf{Y}), \quad \|\mathbf{P}_{\mathbf{M}}(\mathbf{X} - \mathbf{Z})\|_F \le \eta, \\ & \mathbf{Z} = \text{KNN}(\mathbf{P}_{\mathbf{\Omega}}(\mathbf{Y}), \mathbf{\Omega}), \end{aligned} \tag{5}$$

where $\|\mathbf{X}\|_{\mathbf{w},*} = \sum_{i=1}^{\min(m,n)} w_i \sigma_i(\mathbf{X})$, with $\mathbf{w} \ge \mathbf{0}$ ($\mathbf{w} \in \mathbb{R}^{\min(m,n)}$) and $\sigma_i(\mathbf{X})$ is the i-th largest singular value of $\mathbf{X}$. Additionally, $\mathbf{M} \in \mathbb{R}^{m\times n}$ represents a mask matrix where $\mathbf{M}_{ij} = 1$ indicates regions with dense and regularly spaced data suitable for interpolation approaches, while $M_{ij} = 0$ corresponds to areas where the data is sparse or irregular. Meanwhile, $\mathbf{Z}$ is the interpolated matrix derived using the KNN approach, and $\eta \ge 0$ is a tolerance level that balances the trade-off between MC and interpolation. Although WNNM has not been used in RME literature, the singular values of the estimation results using WNNM are proven to be closer to the true values compared to NNM, as shown in Figure 2.

Although Problem (5) is convex and could be addressed using convex optimization tools like CVX [26], its high dimensionality imposes significant computational burdens. Consequently, we introduce an efficient ADMM-based algorithm

in the subsequent section to effectively tackle the IIMC-RME problem.

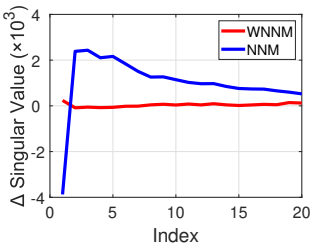

Fig. 2: Comparison of the first 20 singular value differences between WNNM and Ground Truth, as well as between NNM and Ground Truth, as an example of IV-A. Clearly, WNNM leads to almost no difference as indicated by the red curve.

III. Proposed ADMM-Based Algorithm

The ADMM fuses the decomposability of dual ascent with the superior convergence properties of the method of multipliers [21]. We begin by reformulating Problem (5) as follows:

$$\begin{aligned} \min_{\mathbf{X},\mathbf{S},\mathbf{A}} \quad & \|\mathbf{X}\|_{\mathbf{w},*} \\ \text{s.t.} \quad & \mathbf{X}=\mathbf{S}, \quad \mathbf{P}_{\mathbf{\Omega}}(\mathbf{S})=\mathbf{P}_{\mathbf{\Omega}}(\mathbf{Y}), \\ & \mathbf{X}=\mathbf{A}, \quad \|\mathbf{P}_{\mathbf{M}}(\mathbf{A}-\mathbf{Z})\|_F \le \eta, \end{aligned} \tag{6}$$

where $\mathbf{S}\in\mathbb{R}^{m\times n}$ and $\mathbf{A}\in\mathbb{R}^{m\times n}$ are slack variables introduced to decouple $\mathbf{X}$. The augmented Lagrangian function for Problem (6) is $\mathcal{L}(\mathbf{X},\mathbf{S},\mathbf{A},\mathbf{\Gamma},\mathbf{B},\beta,\alpha) = \|\mathbf{X}\|_{\mathbf{w},*} + \frac{\beta}{2}\|\mathbf{X}-\mathbf{S}\|_F^2 + \frac{\alpha}{2}\|\mathbf{X}-\mathbf{A}\|_F^2 + \langle\mathbf{\Gamma},\mathbf{X}-\mathbf{S}\rangle + \langle\mathbf{B},\mathbf{X}-\mathbf{A}\rangle$ where $\mathbf{\Gamma}\in\mathbb{R}^{m\times n}$ and $\mathbf{B}\in\mathbb{R}^{m\times n}$ are the Lagrange multipliers, and $\beta,\alpha>0$ are positive penalty parameters. The optimization problem outlined in Problem (6) can be addressed using the ADMM through the following steps:

1) Updating $\mathbf{X}$*:* Fix the variables as $\mathbf{S}_k$, $\mathbf{A}_k$, $\mathbf{\Gamma}_k$, $\mathbf{B}_k$, β_k, and α_k, then calculate $\mathbf{X}_{k+1}$ as follows:

$$\begin{aligned} \mathbf{X}_{k+1} &= \arg\min_{\mathbf{X}} \Big\{ \|\mathbf{X}\|_{\mathbf{w},*} + \frac{\beta_k}{2}\|\mathbf{X}-\mathbf{S}_k\|_F^2 + \langle\mathbf{\Gamma}_k,\mathbf{X}-\mathbf{S}_k\rangle \\ &\quad + \frac{\alpha_k}{2}\|\mathbf{X}-\mathbf{A}_k\|_F^2 + \langle\mathbf{B}_k,\mathbf{X}-\mathbf{A}_k\rangle \Big\} \\ &= \arg\min_{\mathbf{X}} \Big\{ \|\mathbf{X}\|_{\mathbf{w},*} + \frac{\beta_k+\alpha_k}{2}\|\mathbf{X}-\mathbf{N}_k\|_F^2 \Big\} \\ &= \arg\min_{\mathbf{X}} \Big\{ \|\mathbf{X}\|_{\frac{2}{\beta_k+\alpha_k}\mathbf{w},*} + \|\mathbf{X}-\mathbf{N}_k\|_F^2 \Big\}, \end{aligned} \tag{7}$$

where $\mathbf{N}_k = (\beta_k\mathbf{S}_k + \alpha_k\mathbf{A}_k - \mathbf{\Gamma}_k - \mathbf{B}_k)/(\beta_k+\alpha_k)$.

Then, using [24, Theorem 2], we can derive the closed-form solution for Problem (7):

$$\mathbf{X}_{k+1} = \mathbf{U}S_{\frac{2}{\beta_k+\alpha_k}\mathbf{w}}(\mathbf{\Sigma}_{\mathbf{N}_k})\mathbf{V}^T, \tag{8}$$

where $\mathbf{U}\mathbf{\Sigma}_{\mathbf{N}_k}\mathbf{V}^T$ denotes the SVD of $\mathbf{N}_k$, $\mathbf{S}_{\mathbf{w}}(\mathbf{\Sigma})$ is the generalized soft-thresholding operator with weight vector $\mathbf{w}$:

$$\mathbf{S}_{\mathbf{w}}(\mathbf{\Sigma})_{ij} = \begin{cases} \max(\mathbf{\Sigma}_{ii}-w_i,0), & \text{if} \quad i=j, \\ 0, & \text{otherwise.} \end{cases}$$

Algorithm 1 ADMM-based algorithm for solving problem (5)

Initialize: $\mathbf{X}_1=\mathbf{P}_{\mathbf{\Omega}}(\mathbf{Y})$, $\mathbf{S}_1=\mathbf{X}_1$, $\mathbf{\Gamma}_1=\mathbf{X}_1$, $\mathbf{A}_1=\mathbf{X}_1$, $\mathbf{B}_1=\mathbf{X}_1$, $\beta_1=1$, and $\alpha_1=1$.
do
  Update $\mathbf{X}_{k+1}$ via (8).
  Update $\mathbf{S}_{k+1}$ via (10).
  Update $\mathbf{A}_{k+1}$ via (12) and (13).
  Update $\mathbf{\Gamma}_{k+1}, \mathbf{B}_{k+1}, \beta_{k+1}$ and α_{k+1} via (14), (15), (16) and (17).
  $k \leftarrow k+1$
until $\|\mathbf{X}_{k+1}-\mathbf{X}_k\|_F < \epsilon$;
Output: $\mathbf{X}_{k+1}$

2) Updating $\mathbf{S}$*:* Fix $\mathbf{X}_{k+1}$, $\mathbf{\Gamma}_k$, and β_k, then calculate $\mathbf{S}_{k+1}$ as follows:

$$\begin{aligned} \mathbf{S}_{k+1} &= \arg\min_{\mathbf{S}} \Big\{ \frac{\beta_k}{2}\|\mathbf{X}_{k+1}-\mathbf{S}\|_F^2 + \langle\mathbf{\Gamma}_k,\mathbf{X}_{k+1}-\mathbf{S}\rangle \Big\} \\ &= \arg\min_{\mathbf{S}} \Big\{ \frac{\beta_k}{2}\|\mathbf{S}-(\mathbf{X}_{k+1}+\frac{1}{\beta_k}\mathbf{\Gamma}_k)\|_F^2 \Big\}. \end{aligned} \tag{9}$$

Disregarding the constant terms and setting the values at the observed entries:

$$\mathbf{S}_{k+1} = \mathbf{P}_{\mathbf{\Omega}^c}(\mathbf{X}_{k+1}+\frac{1}{\beta_k}\mathbf{\Gamma}_k) + \mathbf{P}_{\mathbf{\Omega}}(\mathbf{Y}), \tag{10}$$

where $\mathbf{\Omega}^c$ denotes the complement of the set $\mathbf{\Omega}$.

3) Updating $\mathbf{A}$*:* First, we temporarily ignore the constraint $\|\mathbf{P}_{\mathbf{M}}(\mathbf{A}-\mathbf{Z})\|F \le \eta$. Then, with $\mathbf{X}_{k+1}$, $\mathbf{B}_k$, and α_k fixed, we calculate the unconstrained solution $\mathbf{A}_{k+1}$ as follows:

$$\begin{aligned} \mathbf{A}_{k+1} &= \arg\min_{\mathbf{A}} \Big\{ \frac{\alpha_k}{2}\|\mathbf{X}_{k+1}-\mathbf{A}\|_F^2 + \langle\mathbf{B}_k,\mathbf{X}_{k+1}-\mathbf{A}\rangle \Big\} \\ &= \arg\min_{\mathbf{A}} \Big\{ \frac{\alpha_k}{2}\|\mathbf{A}-(\mathbf{X}_{k+1}+\frac{1}{\alpha_k}\mathbf{B}_k)\|_F^2 + \text{Constant} \Big\}. \end{aligned} \tag{11}$$

Ignoring the constant term, we get the solution:

$$\mathbf{A}_{k+1} = \mathbf{X}_{k+1} + \frac{1}{\alpha_k}\mathbf{B}_k. \tag{12}$$

Next, we evaluate the values of $\mathbf{A}_{k+1}$ at the indices set $\mathbf{M}$. If $\|\mathbf{P}_{\mathbf{M}}(\mathbf{A}_{k+1}-\mathbf{Z})\|_F > \eta$, we project $\mathbf{A}_{k+1}$ onto the constraint set using the following projection:

$$\mathbf{A}_{k+1} = \mathbf{P}_{\mathbf{M}^c}(\mathbf{A}_{k+1}) + \mathbf{P}_{\mathbf{M}}(\mathbf{Z}+\eta\cdot\frac{\mathbf{A}_{k+1}-\mathbf{Z}}{\|\mathbf{A}_{k+1}-\mathbf{Z}\|_F}), \tag{13}$$

where $\mathbf{M}^c$ represents the complement of the set $\mathbf{M}$.

Since the constraint $\|\mathbf{P}_{\mathbf{M}}(\mathbf{A}-\mathbf{Z})\|_F \le \eta$ defines a convex set, the global convergence of the ADMM algorithm can be maintained, as outlined in [21, Section 5].

4) Updating $\mathbf{\Gamma}$*,* $\mathbf{B}$*,* β *and* α*:* Fix $\mathbf{X}_{k+1}$, $\mathbf{S}_{k+1}$, and $\mathbf{A}_{k+1}$, we can update $\mathbf{\Gamma}$, $\mathbf{B}$, β and α by the following steps:

$$\mathbf{\Gamma}_{k+1} = \mathbf{\Gamma}_k + \beta_k(\mathbf{X}_{k+1}-\mathbf{S}_{k+1}). \tag{14}$$

$$\mathbf{B}_{k+1} = \mathbf{B}_k + \alpha_k(\mathbf{X}_{k+1}-\mathbf{A}_{k+1}). \tag{15}$$

$$\beta_{k+1} = \rho_1\cdot\beta_k. \tag{16}$$

$$\alpha_{k+1} = \rho_2\cdot\alpha_k. \tag{17}$$

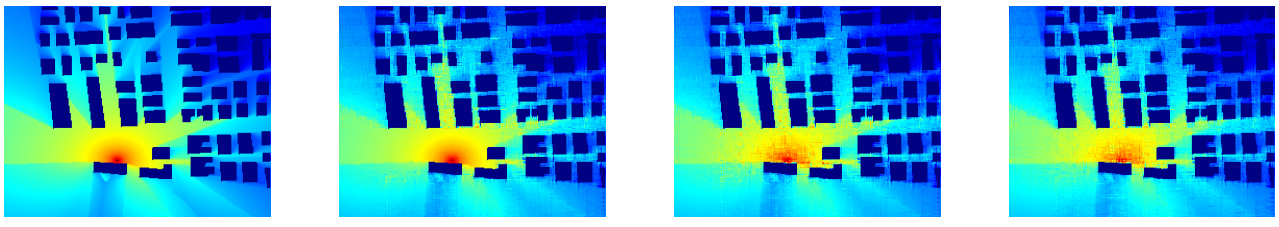

(a) Ground Truth (b) IIMC-RME(NRMSE=0.0298) (c) WNNM (NRMSE = 0.0317) (d) TNNM (NRMSE = 0.0333)

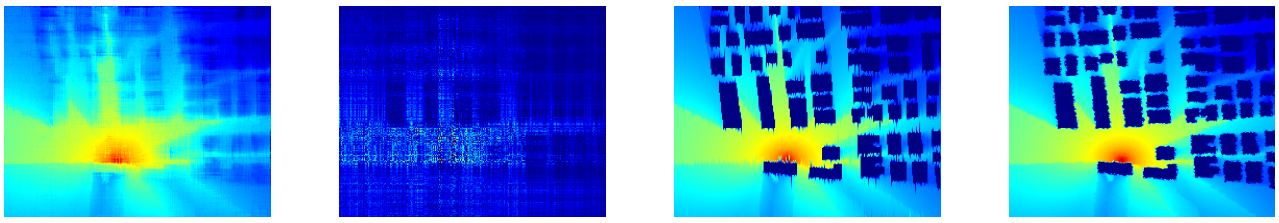

(e) NNM (NRMSE = 0.1561) (f) NMF (NRMSE = 0.2463) (g) LERP (NRMSE = 0.0463) (h) KNN (NRMSE = 0.0490)

Fig. 3: Comparison of different RME approaches for a specific example from the RadioMapSeer dataset [22], where blue represents the minimum pixel value (0), and red represents the maximum pixel value (255).

TABLE I: NRMSE of Different Approaches on Various Datasets

Dataset	IIMC-RME	WNNM	TNNM	NNM	NMF	LERP	KNN
RadioMapSeer	**0.0306**	0.0313	0.0332	0.1491	0.2254	0.0459	0.0481
RMDirectionalBerlin	**0.0348**	0.0440	0.0462	0.1020	0.1628	0.0438	0.0365
Real Data	**0.0072**	0.0816	0.5994	0.0594	0.1171	0.2294	0.1913

The complete procedure is outlined in Algorithm 1. Moreover, the ADMM framework ensures the convergence of Algorithm 1 for solving Problem (5).

IV. Numerical Experiments

In this section, we assess the effectiveness of the proposed approach across various datasets. We compare its performance with benchmark approaches including WNNM, truncated nuclear norm minimization (TNNM) [27], NNM, non-negative matrix factorization (NMF) [28], LERP and KNN.

A. Synthetic Data Experiments

We initially conducted experiments using datasets generated via ray tracing, including RadioMapSeer [22] and RMDirectionalBerlin [23]. In these datasets, path loss values were normalized to a grayscale range from 0 to 255. For all experiments, the sampling ratio is set at 30%, meaning that $|\mathbf{\Omega}|/(mn) = 30\%$ for $\mathbf{X} \in \mathbb{R}^{m\times n}$. The results for a specific example from the RadioMapSeer dataset are presented in Figure 3, with the evaluation metric being the normalized root mean square error (NRMSE).

In Figure 3, it is evident that IIMC-RME provides the best estimation of the ground truth, as shown in Figures 3a and 3b, with the lowest NRMSE. Additionally, IIMC-RME gives a smoother estimation compared to WNNM, TNNM, NNM, and NMF, as seen in Figures 3c - 3f. Among these approaches, NNM still provides a reasonable estimation, though it performs worse than WNNM and TNNM. The NMF method fails completely to provide a good estimate. Figures 3g and 3h indicate that although LERP and KNN produce smoother results than WNNM, TNNM, and NNM, their estimates are more blurred in certain areas, such as dark blue regions. In contrast, IIMC-RME maintains better estimation across all regions, effectively combining the strengths of interpolation and matrix completion for superior performance in the RME problem.

As shown in Table I, the IIMC-RME approach consistently demonstrates superior performance by achieving the lowest NRMSE values compared to other benchmark approaches.

B. Real Data Experiments

We evaluated the proposed algorithm using real data from an office floor at Mannheim University, containing received signal strength indicator (RSSI) values across nine frequency bands [29]. The sampling ratio was set to 40%, and the results are presented in Table I. IIMC-RME achieved the lowest NRMSE among all approaches, demonstrating its superior performance on real data, consistent with its results on synthetic datasets. This significant reduction in NRMSE compared to other approaches highlights IIMC-RME's accuracy in real-world scenarios.

V. Conclusion

In this paper, we introduced IIMC-RME, which effectively integrates the advantages of interpolation and MC approaches. Experimental results from both synthetic and real-world datasets indicate that IIMC-RME surpasses state-of-the-art approaches, consistently achieving the lowest NRMSE across different datasets.

REFERENCES

[1] S. Sorour, Y. Lostanlen, S. Valaee, and K. Majeed, "Joint indoor localization and radio map construction with limited deployment load," *IEEE Transactions on Mobile Computing*, vol. 14, no. 5, pp. 1031–1043, 2015.

[2] R. Shrestha, D. Romero, and S. P. Chepuri, "Spectrum surveying: Active radio map estimation with autonomous uavs," *IEEE Transactions on Wireless Communications*, vol. 22, no. 1, pp. 627–641, 2023.

[3] H. Abou-zeid, H. S. Hassanein, and S. Valentin, "Optimal predictive resource allocation: Exploiting mobility patterns and radio maps," in *2013 IEEE Global Communications Conference (GLOBECOM)*, 2013, pp. 4877–4882.

[4] D. Romero and S.-J. Kim, "Radio map estimation: A data-driven approach to spectrum cartography," *IEEE Signal Processing Magazine*, vol. 39, no. 6, pp. 53–72, 2022.

[5] S. Shrestha, X. Fu, and M. Hong, "Deep spectrum cartography: Completing radio map tensors using learned neural models," *IEEE Transactions on Signal Processing*, vol. 70, pp. 1170–1184, 2022.

[6] S. Timilsina, S. Shrestha, and X. Fu, "Quantized radio map estimation using tensor and deep generative models," *IEEE Transactions on Signal Processing*, vol. 72, pp. 173–189, 2024.

[7] R. Levie, Yapar, G. Kutyniok, and G. Caire, "Radiounet: Fast radio map estimation with convolutional neural networks," *IEEE Transactions on Wireless Communications*, vol. 20, no. 6, pp. 4001–4015, 2021.

[8] X. Zhang, X. Shu, B. Zhang, J. Ren, L. Zhou, and X. Chen, "Cellular network radio propagation modeling with deep convolutional neural networks," in *Proceedings of the 26th ACM SIGKDD International Conference on Knowledge Discovery & Data Mining*, ser. KDD '20. New York, NY, USA: Association for Computing Machinery, 2020, pp. 2378–2386. [Online]. Available: https://doi.org/10.1145/3394486.3403287

[9] V. V. Ratnam, H. Chen, S. Pawar, B. Zhang, C. J. Zhang, Y.-J. Kim, S. Lee, M. Cho, and S.-R. Yoon, "Fadenet: Deep learning-based mm-wave large-scale channel fading prediction and its applications," *IEEE Access*, vol. 9, pp. 3278–3290, 2021.

[10] Z. Wang, L. Zhang, Q. Kong, and K. Wang, "Fast construction of the radio map based on the improved low-rank matrix completion and recovery method for an indoor positioning system," *Journal of Sensors*, vol. 2021, no. 1, p. 2017208, 2021. [Online]. Available: https://onlinelibrary.wiley.com/doi/abs/10.1155/2021/2017208

[11] Y. Hu, W. Zhou, Z. Wen, Y. Sun, and B. Yin, "Efficient radio map construction based on low-rank approximation for indoor positioning," *Mathematical Problems in Engineering*, vol. 2013, no. 1, p. 461089, 2013. [Online]. Available: https://onlinelibrary.wiley.com/doi/abs/10.1155/2013/461089

[12] D. Schäufele, R. L. G. Cavalcante, and S. Stanczak, "Tensor completion for radio map reconstruction using low rank and smoothness," in *2019 IEEE 20th International Workshop on Signal Processing Advances in Wireless Communications (SPAWC)*, 2019, pp. 1–5.

[13] J. Racko, J. Machaj, and P. Brida, "Wi-fi fingerprint radio map creation by using interpolation," *Procedia Engineering*, vol. 192, pp. 753–758, 2017, 12th international scientific conference of young scientists on sustainable, modern and safe transport. [Online]. Available: https://www.sciencedirect.com/science/article/pii/S1877705817326760

[14] Y. Zhang and S. Wang, "K-nearest neighbors gaussian process regression for urban radio map reconstruction," *IEEE Communications Letters*, vol. 26, no. 12, pp. 3049–3053, 2022.

[15] E. J. Candès and B. Recht, "Exact matrix completion via convex optimization," *Foundations of Computational Mathematics*, vol. 9, no. 6, pp. 717–772, 2009.

[16] R. Mazumder, T. Hastie, and R. Tibshirani, "Spectral regularization algorithms for learning large incomplete matrices," *Journal of Machine Learning Research*, vol. 11, no. 80, pp. 2287–2322, 2010. [Online]. Available: http://jmlr.org/papers/v11/mazumder10a.html

[17] T. Hastie, R. Tibshirani, and J. Friedman, *The Elements of Statistical Learning: Data Mining, Inference, and Prediction*, 2nd ed. New York, NY: Springer, 2009. [Online]. Available: https://link.springer.com/book/10.1007/978-0-387-84858-7

[18] H. Sun and J. Chen, "Propagation map reconstruction via interpolation assisted matrix completion," *IEEE Transactions on Signal Processing*, vol. 70, pp. 6154–6169, 2022.

[19] G. Zhang, X. Fu, J. Wang, X.-L. Zhao, and M. Hong, "Spectrum cartography via coupled block-term tensor decomposition," *IEEE Transactions on Signal Processing*, vol. 68, pp. 3660–3675, 2020.

[20] H. Sun and J. Chen, "Integrated interpolation and block-term tensor decomposition for spectrum map construction," 2024. [Online]. Available: https://arxiv.org/abs/2402.17138

[21] S. Boyd, N. Parikh, E. Chu, B. Peleato, and J. Eckstein, *Distributed Optimization and Statistical Learning via the Alternating Direction Method of Multipliers*. Now Publishers Inc., 2011. [Online]. Available: https://doi.org/10.1561/2200000016

[22] Ç. Yapar, R. Levie, G. Kutyniok, and G. Caire, "Dataset of pathloss and ToA radio maps with localization application," *arXiv preprint:2212.11777*, 2022. [Online]. Available: https://arxiv.org/abs/2212.11777

[23] F. Jaensch, G. Caire, and B. Demir, "RMDirectionalBerlin," November 2023. [Online]. Available: https://doi.org/10.5281/ZENODO.10210088

[24] S. Gu, L. Zhang, W. Zuo, and X. Feng, "Weighted nuclear norm minimization with application to image denoising," in *2014 IEEE Conference on Computer Vision and Pattern Recognition*, 2014, pp. 2862–2869.

[25] J. M. Keller, M. R. Gray, and J. A. Givens, "A fuzzy k-nearest neighbor algorithm," *IEEE Transactions on Systems, Man, and Cybernetics*, vol. SMC-15, no. 4, pp. 580–585, 1985.

[26] M. Grant and S. Boyd, "CVX: Matlab software for disciplined convex programming, version 2.1," https://cvxr.com/cvx, Mar. 2014.

[27] Y. Hu, D. Zhang, J. Ye, X. Li, and X. He, "Fast and accurate matrix completion via truncated nuclear norm regularization," *IEEE Transactions on Pattern Analysis and Machine Intelligence*, vol. 35, no. 9, pp. 2117–2130, 2013.

[28] X. P. Li, Z.-L. Shi, Q. Liu, and H. C. So, "Fast robust matrix completion via entry-wise 0-norm minimization," *IEEE Transactions on Cybernetics*, vol. 53, no. 11, pp. 7199–7212, 2022.

[29] T. King, S. Kopf, T. Haenselmann, C. Lubberger, and W. Effelsberg, "Crawdad mannheim/compass (v. 2008-04-11)," 2022. [Online]. Available: https://dx.doi.org/10.15783/c7js3p